Differential mode noise prediction and analysis in single-phase boost PFC for the new frequency range of 9- 150 kHz

Esfetanaj, Naser Nourani; Wang, Huai; Blaabjerg, Frede; Davari, Pooya

Published in:
IEEE Journal of Emerging and Selected Topics in Industrial Electronics

DOI (link to publication from Publisher):
10.1109/JESTIE.2021.3066320

Publication date:
2021

Document Version
Version created as part of publication process; publisher's layout; not normally made publicly available

Differential mode noise prediction and analysis in single-phase boost PFC for the new frequency range of 9- 150 kHz

Naser Nourani Esfetanaj, *Student Member*, *IEEE*, Huai Wang, Senior Member, *IEEE*
, Frede Blaabjerg, Fellow, IEEE and Pooya Davari, Senior Member, IEEE

Abstract— High penetration of power electronics due to the concentration of switching frequency in the range of 9-150 kHz, may create new challenging issues. Currently, regarding the recent version standard (IEC 61000-6-3), there is a lack of enough insight and fundamental studies despite reported Electromagnetic Interference (EMI) noise problems in this frequency range. Hence, this paper proposes a time-frequency analytical modeling method for characterizing Differential Mode (DM) noise in a single-phase Power Factor Correction (PFC) converter in this new frequency range. The provided comparative simulation analysis shows the proposed method's ability to estimate DM noise with a 9-150 kHz frequency range at high accuracy utilizing the double Fourier analysis method. Moreover, the obtained experimental results on a 1 kW single-phase boost PFC converter validate the proposed EMI modeling approach's effectiveness, demonstrating an error of less than 1.8 dB for the considered experimental case studies.

Index Terms— PFC Converter, DM Noise, EMI Modeling, 9-150 kHz.

I. Introduction

Power electronics (PE) converters are penetrating more and more to the power grid due to their crucial role as the energy conversion units. Due to the new technology advancement, most power electronic converters switching frequency is within 2-150 kHz. Their penetration is expected to be dramatically increased in this frequency range. The increasing use of PE converters brings more flexibility to the grid, but it also causes some challenging EMI issues. This is due to their inherent pulse energy conversion characteristics. In fact, the pulse energy conversion of power electronic converters and the necessity of communicating along the power lines lead to serious EMI emission, which may lead the electrical network to be unreliable and inadmissible [1]. For instance, one of the critical areas which may suffer from EMI emission is the smart grid. Many PE converters used in smart grids rely on mains communication systems (MCS) to operate. The generated noise from the PE converter may severely deteriorate MCS communication signals. Thereby maintaining the generated conducted EMI is an essential factor conditioning the proper development of PE based systems. In addition, the multiple working groups in IEC SC77A/CISPR, NASI, and CIGRE standard committee are presently working on the extension of the emission limits below 150 kHz [2]-[5]. Hence, the recent publications and different ongoing standardization activities on the new 2-150 kHz frequency range clearly showing the importance of EMI emission analysis for PWM converters. Notably, it will appear in the current IEC 61000-6-3 [6] as a new frequency range. Moreover, 2-150 kHz range is split into two main frequency bands (i.e., 2-9 kHz and 9-150 kHz) based on the IEC Technical Committee 77A (TC77A) [2]. In addition, CISPR 16-1-1 is classified the 9 kHz -30 MHz frequency range into two main bands as A (9-150 kHz) and B (150 kHz - 30 MHz) [7]. Hence, Fig. 1. shows an overview of the classified EMI frequency ranges according to IEC. There is no general standard covering the 2-150 kHz frequency range. Therefore, there is a lack of systematically understanding the noise propagation through the power network within this frequency range [8].

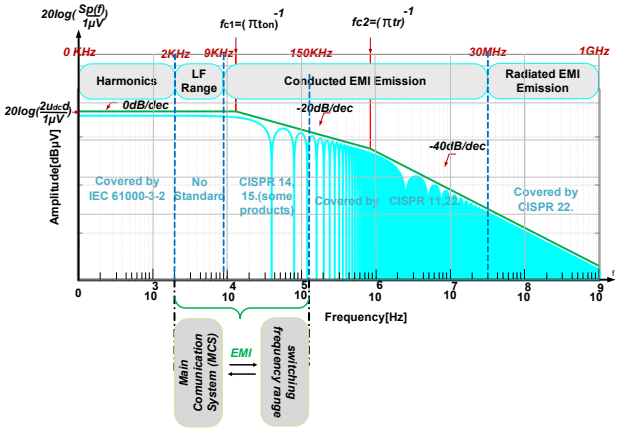

Fig. 1. Overview of the classified EMI frequency ranges according to IEC with corresponding trapezoidal waveform frequency spectra, (u_{dc} =400, f_s = 20 kHz, t_r = t_f = 400 ns, d = 0.5).

To better understand PE converter's frequency behavior, a suitable modeling approach is necessary to estimate DM EMI noise levels and design proper DM EMI filters to comply with recommended standards. Notably, the lack of general standards within 9 -150 kHz, lead to a lack of power converters characteristic models in this frequency range. Hence, providing this model can characterize the influence parameters, which are used to simplify to model at the system-level study. Many simulation-based modeling approaches have been introduced, but the analytical-based modeling approach is essential to improve computation time and to scale it up for system-level. In addition, to get a simplified EMI model within 2-150 kHz, it is necessary to identify salient parameters to reduce the model order and complexity.

Up to now, EMI modeling and analysis have been considered for above 150 kHz. For instance, in [9]-[11] high-

Manuscript received xxx; revised xxx; accepted xxx. Date of publication xxx.

N. Nourani Esfetanaj, H. Wang, F. Blaabjerg, and P. Davari are with the Department of Energy Technology, Aalborg University, 9220 Aalborg, Denmark (e-mail: nne@et.aau.dk; hwa@et.aau.dk; fbl@et.aau.dk; pda@et.aau.dk.

frequency modeling of power converters for investigating EMI emission is introduced based on Thevenin and Norton equivalent circuit models above, then 150 kHz. Several types of EMI filters, such as DM, common mode (CM), and CM+DM filters, have been presented for above 150 kHz range [9], [12]-[15] according to recommended standard limits [7], [16], [17]. The majority of modeling approaches which have been focused on above 150 kHz frequency range EMI analysis are simulation-based. All introduced methods have high complexity, due to the presence of parasitic from components and PCB layout. Hence, all methods suitable for high-frequency EMI modeling (i.e., >150 kHz) can be used to estimate the EMI below 150 kHz frequency range as well as, however with the cost of high complexity and high computation time.

Consequently, only a few articles based on simulations and experiments have been focusing on EMI issues below 150 kHz [1], [8], [18]-[24]. Hence, this paper aims at proposing an analytical-based modeling approach for DM EMI noise in this frequency range. Since PFC converters have become popular solutions in most power electronic applications due to fulfilling harmonic standards and increasing power density [25], an analytical model for a PFC converter is proposed in this paper. The proposed model is developed based on time-frequency domain analysis representing the power converter behavior utilizing its switching function as the main noise source and its closed loop impedance for EMI estimation. A reduced-order analytical DM EMI model is developed for the 9-150kHz regime based on the following assumptions:

- Parasitic component effects are negligible.
- Rise and fall times of switching waveforms produce negligible harmonics and can be ignored.

Based on these assumptions, the proposed analytical modeling technique is valid for the 9-150 kHz frequency range, and it can be extended for higher frequency ranges when the effects of devices and components parasitics are included. That is why majority of modeling methods applied for high frequency EMI modeling are based on simulations and semi-practical models due to the complex behavior of different components and dependency of the EMI behavior on power converter design. Consequently, the parasitic effect is not modeled in this paper, as long as the effects of them are negligible. Hence, this paper's main goal is to propose a suitable order reduction method at low-frequency ranges, considering the power converters with different topology and modulation. Moreover, only a few analytical-based approaches are introduced suitable for differential mode noise as in [26] which is referred to as a "conventional approach" in the paper for comparative study. Based on the providing comparative study, it has been shown that the conventional approach is only suitable for EMI filter designing or sizing as it only predicts the first peak of the emission with high accuracy. However, the proposed method characterizes the generation emission of the power converter within 9-150kHz based on the double Fourier analysis and closed-loop impedance. The proposed modeling approach can be used for EMI filter design considering its accurate noise emission estimation, though this is not the main purpose of the model. Hence, the conventional approach is used to compare the proposed method to highlight the proposed method's accuracy and suitability for filter designing. Consequently, this paper's main focus is not EMI filter designing, but the main novelty of this work is EMI emission modeling of boost PFC within the 9-150 kHz frequency range and not just the first appearing peak.

Furthermore, in the new frequency range, the DM noise is more critical than CM noise due to the small size of the parasitic capacitor, which limits the EMI level under standard criteria [3]-[5]. It is valid in most applications except for some particular applications like motor drives [23]. Notably, the effect of Line Impedance Stabilization Network (LISN), EMI receiver, and EMI filters are considered as well. The analytical equivalent circuit of the boost PFC has been presented in [22]. The model is extended in this work by designing proper DM EMI filters, and the analytical approach is updated in the presence of EMI filter by the Middlebrook theory. Comparative analysis with a conventional analytical modeling approach is provided, and it is shown that the proposed method can simplify estimate all DM noises within 9 - 150 kHz with high accuracy utilizing double Fourier analysis. In addition, the sampling and partial power effects on closed-loop input impedance have been investigated. Additional experimental with considering the EMI filter has been provided in this research.

This paper is structured as follows. Section II describes the analytical time-frequency EMI modeling based on the converter's developing switching function as Thevenin noise voltage and closed-loop input impedance as equivalent circuit impedance. In the following, the closed-loop input impedance modeling is developed considering the effect of sampling frequency, low pass filter on the controller, and partial loading effect. Furthermore, the equivalent circuit updates from the filter effect by Middlebrook theory in (Section II-A). Moreover, the LISN and EMI receiver analytical models are presented in Section II-B. In addition, the design procedure of the EMI filter is presented in Section II-C for band A following the proposed and conventional methods. The considered conventional modeling method is briefly explained in Section II-D. Section III is dedicated to comparative analysis supported by simulation and experimental results. Finally, conclusions are drawn in Section VI.

II. TIME-FREQUENCY DOMAIN MODELING

Fig. 2 shows the block diagram of the studied system including the power stage of a boost PFC, LISN, EMI receiver and EMI filter. In this section, first the proposed analytical modeling approach is described and later a conventional modeling approach [26] for the sake of comparison is briefly explained.

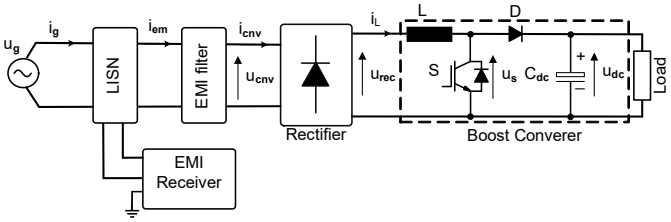

Fig. 2. Block diagram of a single-phase boost PFC converter including LISN, EMI receiver and EMI filter.

A. Proposed Time-Frequency Domain Model

As it is shown in Fig. 3, the proposed method's principal idea is based on developing Norton equivalent circuit model of the converter. Thereby, in order to develop this model, the power converter should be characterized as a noise source and its closed-loop impedance.

A.1 DM EMI noise source model

As it is well-known, the main DM noise source is due to the switching action. Therefore, the first step is to model the voltage across the power switch in the converter. Fig. 4 exemplifies the waveform of the voltage across the switch having a trapezoidal shape and a periodic pulse train, including the rise and fall times. For frequency analysis, Fourier series coefficients can be calculated from (1), by considering equal rise and fall times:

$$S_p(f) = 2u_{dc}d\frac{\sin(n'\pi ft_{on})}{n'\pi ft_{on}}\frac{\sin(n'\pi ft_r)}{n'\pi ft_r} \tag{1}$$

where u_{dc} is the amplitude of the waveform, d is the duty cycle, n' is harmonic order, t_{on} is the pulse width, f the frequency, t_r is rise time [27]. The frequency spectrum of a trapezoidal waveform has been shown in Fig. 1. The second corner frequency depends on rising or falling times. Thereby, in order to see the effect of the rise or fall time on the EMI noise below 150 kHz frequency range, this transition time should be larger than 2.15 µs, which is not the case for most power semiconductor switches as they operate much faster. Therefore, for the sake of simplicity, since the focus is on frequencies below 150 kHz, an ideal pulse waveform is considered. The Fourier series of it can be expressed as

$$S_p(f) = 2u_{dc}d\frac{\sin(n'\pi ft_{on})}{n'\pi ft_{on}} \tag{2}$$

In most grid-connected applications, such as boost PFC, due to employed modulation strategy the duty cycle is not fixed. In order to consider the effect of modulation, in [26] a time-domain modeling method is introduced to calculate the converter input noise current. In this work, the impact of the modulation strategy is modeled through a double Fourier analysis. Therefore, in order to develop the switching function of the voltage across the switch, the applied modulation under continuous conduction mode (CCM) operation, as shown in Fig. 5 is considered. Hence, the frequency-domain function of the voltage across the switch can be presented as (3), where it includes a dc offset rate, baseband, carrier and sideband harmonics

$$\begin{aligned} u_s(t) &= \frac{a_{00}}{2} + \sum_{n=1}^{\infty}[a_{0n}\cos(n\omega_g t) + b_{0n}\sin(n\omega_g t)] \\ &+ \sum_{m=1}^{\infty}[a_{m0}\cos(m\omega_{sw}t) + b_{m0}\sin(m\omega_{sw}t)] \\ &+ \sum_{m=1}^{\infty}\sum_{\substack{n=-\infty \\ n\neq 0}}^{\infty} a_{mn}\cos(\left[m\omega_{sw} + n\omega_g\right]t) + b_{mn}\sin(\left[m\omega_{sw} + n\omega_g\right]t) \end{aligned} \tag{3}$$

where m and n represent the carrier index and based band index variables, respectively, which are integer multiples of the fundamental component. In addition, ω_{sw} and ω_g are showing fundamental and carrier angular frequencies. Moreover, a_{0n}, b_{0n}, a_{m0}, b_{m0}, a_{mn}, and b_{mn} are indicated the Fourier coefficients,

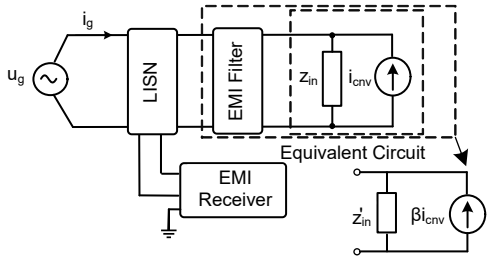

Fig. 3. Norton equivalent circuit of the simplified boost PFC converter with EMI filter.

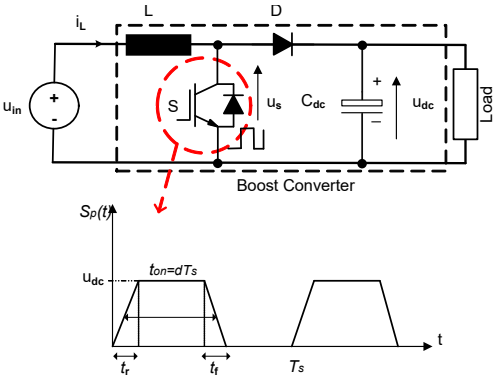

Fig. 4. Trapezoidal switching waveform approximation (voltage waveform across the switch) in boost converter for constant duty cycle.

which should be computed from the double Fourier series of the voltage across [28]. Thereby, it is presented in (4)

$$a_{mn} + jb_{mn} = \frac{1}{2\pi^2}\int_{-\pi}^{+\pi}\int_{-\pi.M.|\cos(y)|}^{\pi.M.|\cos(y)|} u_{dc}e^{j(m.x+ny)}dxdy \tag{4}$$

whereby the u_{dc} is the output dc voltage, M the modulation index written as

$$M = \frac{u_g}{u_{dc}} \tag{5}$$

Moreover, by neglecting rise or fall time effects on 2-150 kHz based on the (1) and (2), pulse voltage across the switch can be considered as an ideal pulse with a variable duty cycle. Hence rise or fall time effect is ignored from (4) to calculate the Fourier coefficients. Notably, the double Fourier's integral domain is determined by considering the modulation scheme in Fig. 5. Selective values of the index variables m and n will be evaluated from (4) by considering the modulation's integer multiples and fundamental frequency. Hence, the dc component can be found with replacement $m = n = 0$ in the (4) as

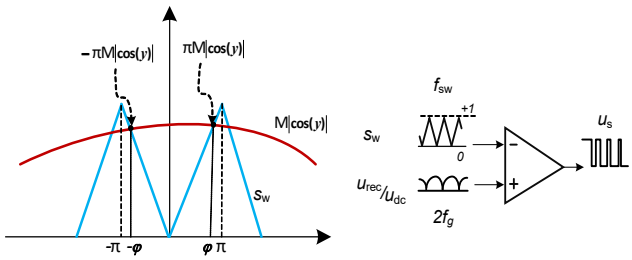

Fig. 5. Illustration of single-phase boost PFC modulation scheme in CCM.

$$a_{00} + jb_{00} = \frac{a_{00}}{2} = \frac{2Mu_{dc}}{\pi} \tag{6}$$

Notably, baseband and fundamental harmonics can be achieved by replacing the index variable of $m = 0$ in (4) as

$$a_{0n} + jb_{0n} = \frac{Mu_{dc}}{\pi}(-ni + 2e^{\frac{n\pi i}{2}} + ine^{n\pi i})\frac{-e^{-n\pi i}(1+e^{n\pi i})}{n^2-1} \tag{7}$$

Furthermore, carrier harmonics is determined by substituting the index variable of $n = 0$ in (4) as

$$a_{m0} + jb_{m0} = \frac{8u_{dc}}{\pi^2}\frac{1}{m}\sum_{\substack{k=1\\k=odd}}^{\infty}\frac{J_k(m\pi M)}{k} \tag{8}$$

Subsequently, by using the index variables, $m \neq 0$, $n \neq 0$ in (4), sideband harmonics, defined for either side of the main carrier harmonics, is

$$a_{mn} + jb_{mn} = \frac{2.u_{dc}}{\pi^2}\frac{1}{jm}\times \sum_{k=1}^{\infty} J_k(m\pi M)(j^k - j^{-k})\left(\frac{(\sin(\frac{k-n}{2})\pi)}{k-n} + \frac{(\sin(\frac{k+n}{2})\pi)}{k+n}\right) \tag{9}$$

Finally, the frequency spectrum of the noise source is obtained by using the (7) - (9). Further, in order to determine the noise source at converter input side, u_s should be updated by the full-bridge diode rectifier influence. Hence, Fourier frequency analysis of the full-bridge rectifier can be calculated by considering a square waveform signal of switching function. The frequency spectrum of the full-bridge diode rectifier is

$$u_{fd}(t) = \sum_{\substack{h=1\\h=odd}}^{\infty}\frac{2}{h\pi}\sin(\frac{h.\pi}{2})\cos(\omega_g ht) \tag{10}$$

Consequently, Thevenin voltage as the noise voltage model from the grid side point of view in Fig. 3 is taken by employing (11)

$$u_{th}(t) = u_{fd}(t)u_s(t) \tag{11}$$

Finally, Norton current can be achieved after calculating the converter closed-loop input impedance.

A.2 Closed loop input impedance

In this part, the closed-loop input impedance modeling is presented. More designations details about closed-loop input impedance modeling and its frequency behavior have been addressed in [29]. A closed-loop block diagram of a single-phase boost PFC converter is shown in Fig. 6. Since this paper focuses on below 150 kHz, it is not necessary to consider the effect of layout and components high-frequency behavior. However, closed loop impedance model can be calculated based on a large signal model by employing (12)

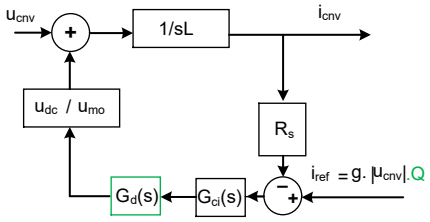

Fig. 6. Block diagram representing input current dynamics of boost single-phase PFC converter.

$$z_{in} = \frac{u_{cnv}}{i_{cnv}} = \frac{sL + \frac{R_s}{u_{mo}}(u_{dc}G_{ci})}{1 + \frac{1}{u_{mo}}(gu_{dc}G_{ci})} \tag{12}$$

where u_{mo} is the peak-to-peak value of the PWM signal and g is a fixed value, and it can be calculated from $g = p_{in}/v_{in}^2$ that p_{in} and v_{in} are defined as the input power and input voltage respectively. Moreover, it is necessary to add a low pass filter in the current reference to ensure system stability in all operating conditions [30] and decrease zero-crossing distortion [29]. The effect of low pass filter on the current reference is not negligible at high-frequency and It must be applied to the closed-loop input impedance model [29]. Therefore, i_{ref} in Fig. 6, should be replaced by $i_{ref} = g.Q.|u_{cnv}|$. Hence, the low pass filter transfer function is presented by (13)

$$Q \approx \frac{1}{1 + \frac{s}{\omega_z}} \tag{13}$$

ω_z is mostly defined as (14)

$$\omega_z = 2\pi f_z \tag{14}$$

where f_z is filter cut-off frequency. Furthermore, by including the low pass filter, the closed-loop input impedance can be estimated by only boost inductor impedance in the frequency range of 9-150 kHz, as it can be seen in Fig. 7. It is a reasonable simplification in order to reduce the model order and computation time, which is important for system-level analysis. On the other hand, the control parameters are a function of its bandwidth, and since the bandwidth is typically limited up to 9 kHz, they can be neglected. Thereby, the closed-loop input impedance can be simplified by (15)

$$z_{in} = \frac{sL + \frac{R_s}{u_{mo}}(u_{dc}G_{ci})}{1 + \frac{1}{u_{mo}}(gQu_{dc}G_{ci})} \approx sL \tag{15}$$

Fig. 7 illustrates the low pass filter effects on closed-loop input impedance behavior, which makes the impedance behavior matching the boost inductor characteristics for higher frequency ranges, which suited the 9 – 150 kHz frequency range of interest.

A.2.1 Sampling effect on closed loop input impedance

To investigate the microcontroller sampling effect on the model, its transfer function G_d is defined as below and needs to be included in the closed loop impedance model:

$$G_d = e^{-sT_d}, (T_d = 1.5T_{sw}/k, k = T_{sw}/T_s) \tag{16}$$

where T_{sw} is switching time, T_s is sampling time, and T_d is the introduced time delay in the control loop. The term k refers to the ratio between switching time and sampling time, for example, when both of them are equal, k should be chosen as one. Therefore, the closed-loop impedance model considering the sampling time can be written as

$$z_{in} = \frac{u_{cnv}}{i_{cnv}} = \frac{sL + \frac{R_s}{u_{mo}}(u_{dc}.G_d.G_{ci})}{1 + \frac{1}{u_{mo}}(g.Q.u_{dc}.G_{ci}.G_d)} \approx sL \tag{17}$$

if f > 9 kHz then it can be approximated as sL. Fig. 8 illustrates a closed-loop input impedance behavior with considering sampling and low pass filter effects into the model in Fig. 6. Moreover, the closed-loop impedance model with sampling $2f_{sw}$ and $5f_{sw}$ with a low pass filter from equation (17) is presented in Fig. 8. Further, it is clear that the closed-loop by consideration of the low pass filter and sampling $2f_{sw}$ is confirmed by simulation result, which is done using PLECS. In order to investigate the effect of sampling frequency on input impedance behavior, Fig. 9 shows two simulated EMI results based on the PLECS simulation with considering the sampling frequency of $2f_{sw}$ and without it. As it can be seen from Fig. 9, the effect of sampling can be ignored from the closed-loop impedance modeling, because of the low effect in the EMI simulation. One can notice that from Fig. 8, the resulting sampling effects strongly depend on the switching frequency chosen. This may increase the estimated error on the EMI levels. Hence, Fig. 10 illustrates simulated low frequency EMI considering sampling frequency for a case study with 10 kHz as switching frequency. As shown in Fig. 10, the error between two simulation cases, is increased up to 1.8 dB. As a consequence, the sampling transfer function should be considered in input impedance modeling when switching frequency is chosen under 20 kHz.

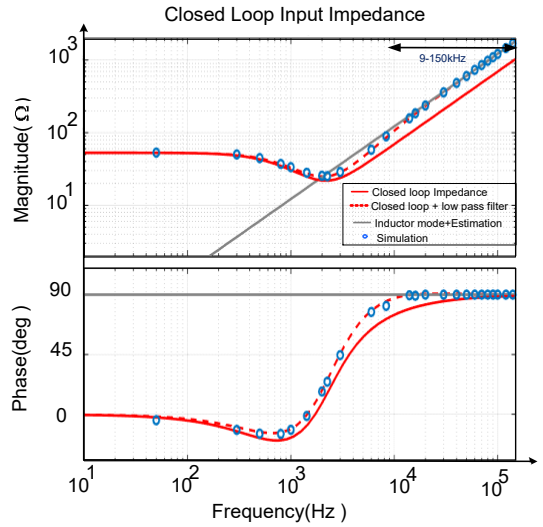

Fig. 7. Closed-loop impedance behavior following equation (12) including the effect of low pass filter versus boost inductor-based model following (15) and simulation results from PLECS (i.e., switching model).

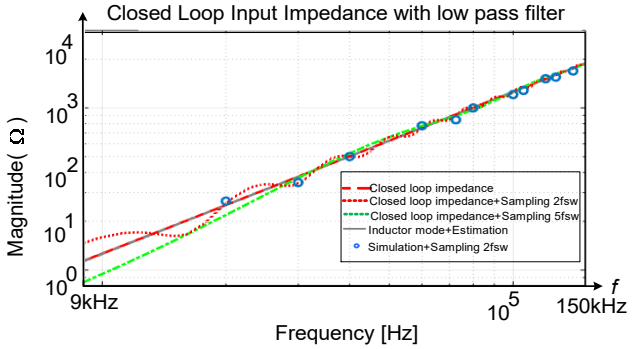

Fig. 8. Closed-loop impedance behavior based on simplified boost inductor model given by (15), the developed model in (17) with sampling $2f_{sw}$ and $5f_{sw}$ and simulation using PLECS software with $2f_{sw}$ sampling. All scenarios are with a low pass filter.

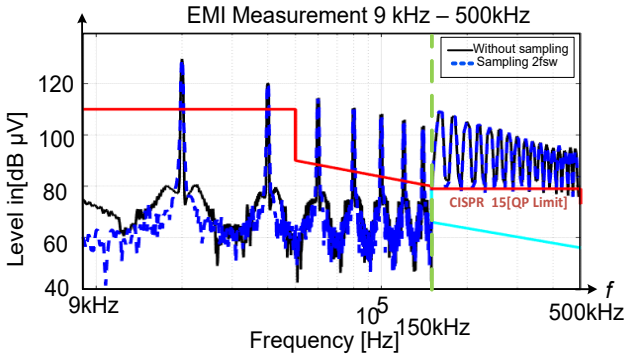

Fig. 9. EMI simulation 9 kHz – 500 kHz by considering the sampling transfer function (sampling frequency is equal two times of switching frequency) for case with f_{sw} = 20 kHz.

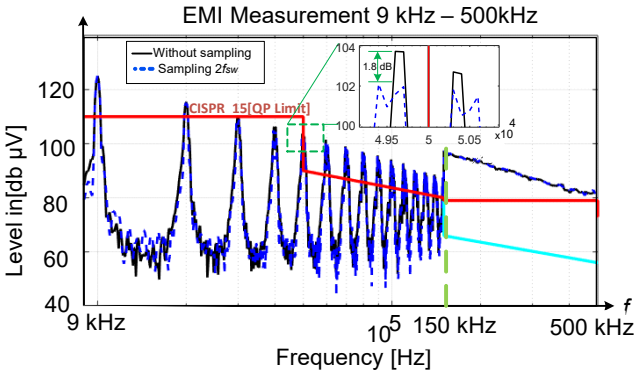

Fig. 10. EMI simulation 9 kHz - 500 kHz with considering of sampling transfer function (sampling frequency is equal two times of switching frequency) with including zoom parts to do a clarify comparison for case with f_{sw} = 10 kHz.

A.2.2 Partial power effect on closed loop input impedance

This part investigates the effect of output power change on the input closed loop impedance. Hence, considering (12), the closed-loop impedance depends on the power rating with g, and it can be changed in the converter's operation mode. However, as shown in Fig. 11, loading conditions can be neglected in the impedance behavior above current controller bandwidth (i.e., > 9 kHz). Therefore, the closed-loop input impedance can be estimated by only the boost inductor impedance in the frequency range of 9-150 kHz, which is typically beyond the current controller bandwidth (see Figs. 7, 8 and 11). Finally, in this paper, there are two case studies with different inductor sizes, which are shown in Fig. 12. As it can be seen from the Fig. 12, closed-loop input impedance has been simplified to inductor impedance after 9 kHz, and it can be changed by changing inductor size. Notably, the dependency of closed-loop input impedance to the inductor size after the 9 kHz is the main purpose of Fig.12 based on the (15).

A.3 Norton current model

Consequently, as mentioned in the above, Norton current as noise source model of the equivalent circuit can be achieved from the Thevenin voltage divided to the closed-loop input impedance

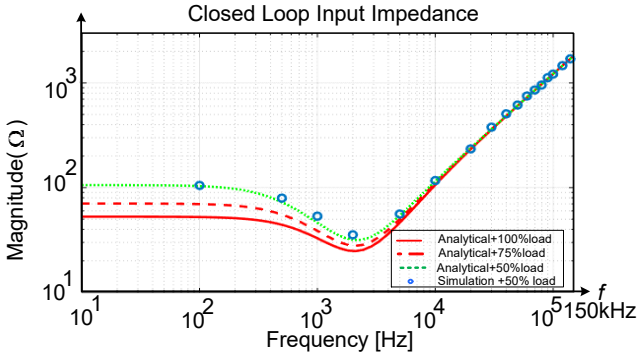

Fig. 11. Effect of output power level on close loop impedance behavior based on model from (15), and simulation using PLECS software with 50% of load. All scenarios are with low pass filter.

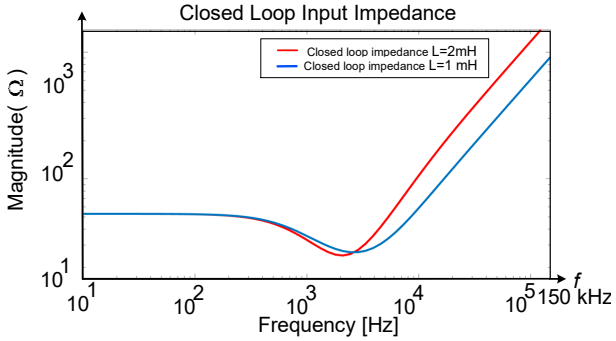

Fig. 12. Effect of inductor changing on close loop impedance behavior based on (15).

$$i_{cnv} = \frac{u_{th}}{z_{in}} \tag{18}$$

Therefore, the Norton equivalent circuit model for the single-phase boost PFC converter is displayed in Fig. 3 by closed-loop input impedance and Norton current source, which is manifested in the above. In addition, The EMI filter for noise level limitation should be coupled to the Norton model.

A.4 Update model with EMI filter effects

The design process of the EMI filter will be given for band A in part D of this section. The general structure of the EMI filter is shown in Fig. 13. However, modifying the equivalent circuit with EMI filter is done by the Middlebrook theory. This part aims at presenting an equivalent circuit model, including converter and EMI filters, to simplify the modeling of low-frequency EMI. Furthermore, more details of this theory have been discussed in [31]. Hence, first of all, if we consider the closed-loop input impedance of the boost PFC converter as an extra element component that connects on the secondary point of the EMI filter. According to Middlebrook theory, the updated input impedance from the grid side with attending of EMI filter, can be calculated from (19)

$$z'_{in} = z_{in\_filter} \cdot \frac{1+\frac{z_n}{z_{in}}}{1+\frac{z_d}{z_{in}}} \tag{19}$$

Where, $z_{in\ filter}$ is the input impedance of the EMI filter in the grid side without visiting extra impedance in secondary. Moreover, z_{in} is closed-loop input impedance, which is presented before. z_n and z_d, which are defined in Middlebrook theory. The input impedance of the EMI filter when the second part is a short circuit, is given by

$$z_{in\_filter} = z_{C_{DM}} + 2(z_{L_{DM}} + \frac{R_{DM}.z_{L_{DM}}}{R_{DM}+z_{L_{DM}}}) \tag{20}$$

According to the Middlebrook theorem, the relation between two input and two output signals in the linear system can be defined by (21).

$$\begin{cases} u_{01} = A_1 u_{i1} + A_2 u_{i2} \\ u_{02} = B_1 u_{i1} + B_2 u_{i2} \end{cases}, u_{02} = v, u_{i2} = i \tag{21}$$

Where u_{01} and u_{02} are output signals, coefficients of A_1, A_2, B_1, and B_2 are transfer functions. Finally, u_{i1} and u_{i2} are input signals. For the sake of brevity, they are not explained in detail in this paper, and the reader is referred to [31] for more information.

Where z_n is defined as an impedance view from an extra element side in theorem when another side is a short circuit. Thereby, it can be obtained as below:

$$\frac{v}{i}\Big|_{u_{01}=0} = z_n\Big|_{u_{01}=0} = \frac{A_1B_2 - B_1A_2}{A_1} = 2(z_{L_{DM}} + \frac{R_{DM}.z_{L_{DM}}}{R_{DM}+z_{L_{DM}}})\Big\|z_{C_{DM}} \tag{22}$$

Notably, z_d is determined as an impedance view from the extra element side in theorem when the extra element side is open circuit.

$$\frac{v}{i}\Big|_{u_{i1}=0} = z_d\Big|_{u_{i1}=0} = B_2 = z_{C_{DM}} \tag{23}$$

Hence, Fig. 14. shows a closed-loop impedance model with and without considering of EMI filter. Moreover, for calculating a closed-loop with EMI filter, an analytical closed loop from (15) is updated by Middlebrook theory. In addition, simulation results are used to validate Middlebrook output. In the next step,

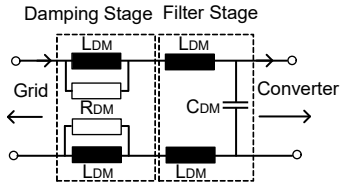

Fig. 13. DM EMI filter configuration with one filtering stages and one damping stage.

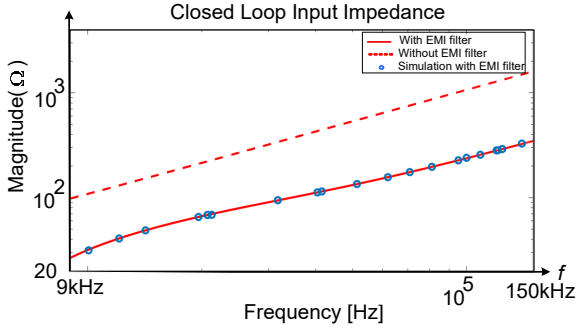

Fig. 14. Closed-loop input impedance model without EMI filter based on (15), with considering of EMI filter base on the equation (19) and simulation for considering EMI filter from PLECS software.

a modified Norton current with considering of EMI filter should be investigated. The relation between Norton current with and without of EMI filter is calculated by

$$\frac{i_{em}}{i_{cnv}} = \beta \tag{24}$$

Where i_{cnv} is Norton current without EMI filter, i_{em} is Norton current with considering EMI filter, β as again, and it can be calculated by (24). The relation between input EMI filter current and Norton current can be calculated from

$$\frac{i_1}{i_{cnv}} = \frac{z_{in}}{z_{in} + z_n} \tag{25}$$

Furthermore, the relation between input and output current of the EMI filter can be calculated as

$$\frac{i_{em}}{i_1} = \frac{z_{C_{DM}}}{2(z_{L_{DM}} + \frac{R_{DM}.z_{L_{DM}}}{R_{DM} + z_{L_{DM}}}) + z_{C_{DM}}} \tag{26}$$

i_{em} as final Norton current can be determined with the implementation of (25) and (26) into (24)

$$\beta = \frac{z_{C_{DM}}}{2(z_{L_{DM}} + \frac{R_{DM}.z_{L_{DM}}}{R_{DM} + z_{L_{DM}}}) + z_{C_{DM}}} . \frac{z_{in}}{z_{in} + z_n} \tag{27}$$

β is the relation between Norton current with and without the EMI filter. Finally, the equivalent circuit model considering the EMI filter, as shown in Fig. 2 is ready to be analyzed and thereby investigate the EMI model.

B. LISN and EMI receiver analytical model

According to CISPR 16 standard [11], LISN is considered between converter and grid, as shown in Fig. 15(a). It can guarantee the reproducibility of the measurements, fix the impedance for the EMI receiver branch, and finally decouple the equipment under test from the grid. Furthermore, due to the measurement noise level, the EMI receiver can be connected to LISN. More informations about LISN and EMI receiver are presented at [8]. As explained before, Norton noise current through into the LISN, and then EMI receiver can measure the noise emission as a voltage signal. Hence, the EMI receiver and LISN model should be attached to the analytical models in order to estimate the EMI noise level. Fig. 15(b) shows the transfer function between LISN input current and EMI receiver voltage. It has to be noticed that this transfer function should be added as an analytical form on the proposed method. In addition, the relationship between input current LISN and EMI receiver branch by considering the EMI filter is presented in (28).

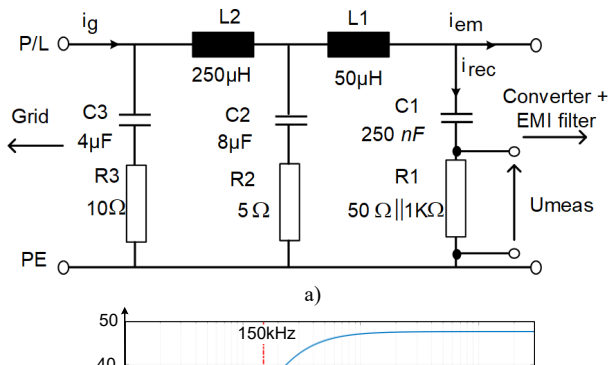

$$i_{rec} = \frac{C}{D} i_{em} \tag{28}$$

C and D are defined in (29) and (30), respectively.

$$C = L_1L_2C_1C_2s^4 + R_2C_1C_2(L_2 + L_1)s^3 + C_1(L_2 + L_1)s^2 \tag{29}$$

$$D = C_1C_2(R_2L_1 + L_2L_1)s^4 + C_1C_2(L_2R_1 + L_2)s^3 + (L_1C_1 + L_2C_2 + L_2C_1 + R_1R_2C_2C_1)s^2 + (R_1C_1 + R_2C_2)s + 1 \tag{30}$$

Moreover, i_{cnv} can be used instead of i_{em} in (28) for measurement of the EMI level without considering EMI filter. In addition, the EMI receiver voltage noise is

$$U_{meas} = R_1 i_{rec} \tag{31}$$

According to CISPR 16 standard for Band A, the bandwidth of the EMI receiver filter should be kept as 200 Hz. Furthermore, a 4th order Butterworth filter is employed for modeling of this filter, and the EMI is determined by sweeping the RBW filter in the frequency range of band A. By utilizing the EMI peak measurement equation [22], [26], the EMI receiver can be modeled by

$$U_{\max}[dB\mu V] = 20\log[1/\mu V \sum_{f=MB-\frac{BW}{2}}^{f=MB+\frac{BW}{2}} U_{meas}(f) \cdot RBW(f)] \tag{32}$$

C. Designing EMI Filter

In this part, the design process of the EMI filter will be discussed. The main objective is to design a suitable filter that can limit the recommended standard's EMI level. Moreover, the EMI filter performance depends on its passive components such as inductors and capacitors. Hereby, the overall prototype of one stage EMI filter has been depicted in Fig. 13. Notably, it is common to utilize the CM choke's leakage inductance as L_{DM} to meet frequencies above 150 kHz standards in the practical EMI filter designing [12]. However, suppress the noise emission below 150 kHz, the CM choke leakage inductance may not be enough. Therefore, additional DM inductor needs to be designed and considered for the DM filter for mitigating below 150 kHz frequency range. In addition, the filter design is dependent on the required filter attenuation *Attreq*, which can

TABLE I
CASE STUDY SPECIFICATION

Symbol	Parameter	Value	Unit
u_g	Grid phase voltage	230	Vrms
f_g	Grid frequency	50	Hz
L	DC link inductor	2,1	mH
f_{sw}	Switching Frequency	20,40	kHz
C_{dc}	DC link capacitor	500	μF
U_{dc}	Output voltage	400	V
P_o	Output power	1	kW

be found by analyzing the detected QP voltage (U_{max}) with the CISPR QP limits, which are presented in (33)

$$A_{tt_{req}}(f)[dB] = U_{\max}(f)[dB\mu V] - CISPR_{\lim it}(f)[dB\mu V] + M\arg in[dB] \quad (33)$$

where Att_{req} is the quantity of noise that filters should be damping, and also, U_{max} is the maximum peak of the spectrum, which can be achieved from the proposed analytical model; $CISPR_{limit}$ can be found from the standard as shown in Fig. 1. In addition, 6 dB margin is considered for covering the component tolerances and parameter shifts due to degradation. However, for one-stage EMI filter size of inductor and capacitor can be calculated from the following equation

$$A_{tt}(f_{sweep}) \geq \frac{2L^2_{DM}C_{DM}(j2\pi f)^3 + 4L_{DM}R_{DM}C_{DM}(j2\pi f)^2 + L_{DM}(j2\pi f) + R_{DM}}{R_{DM} + L_{DM}(j2\pi f)} \quad (34)$$

$$= A_{tt_{EMI\_Filter}(f_{sweep})}$$

D. Conventional Time-Frequency Domain Modeling [26]

In order to highlight the performance of the proposed analytical modeling approach, a conventional analytical method introduced in [26] is briefly presented here, and it has been considered for a comparative analysis in the next section. Notably, this method was introduced for DM noise estimation for > 150 kHz frequency ranges, and it is adapted here for the new frequency range of 9 - 150 kHz by including frequency behavior of LISN network. As discussed before, in boost PFC case study, there is a modulation with variable duty cycle. The proposed model uses a double Fourier for the applied modulation effect on the model, but the conventional model presented an analytical time-domain formulation base on the current ripple model. Furtheremore, it is a simplified method for designing an EMI filter. More details of the analytical EMI Time-domain have been given in [26], and in the following, the general noise RMS current is given by (35)

$$I^2_{noise,rms} = \frac{-64\alpha + 12\pi + 9\alpha^2\pi}{18\pi}.\alpha^2.\Delta I^2_{L,CCM,\max} \quad (35)$$

$\Delta I_{L,CCM,\max}$ is as the chosen maximum inductance current ripple, α is defined by

$$\alpha = \frac{U_{in}}{U_0} \quad (36)$$

where U_{in} is the peak of input ac voltage, and U_o is output dc voltage. In [26], this method is used for EMI noise estimation above 150 kHz. For using this method under 150 kHz, note that Fig. 15.b gives the relation between U_{meas} and $I_{\text{noise,rms}}$ and it is not fixed in the frequency range between 9-150 kHz. Hence, C/D is applying a correction factor in the analytical model noise. Finally, U_{meas} as a noise voltage in EMI receiver input is presented by

$$U_{meas} = (50 \,||\, 1K\Omega).\frac{C}{D}.I_{noise,rms} \quad (37)$$

In addition, the estimated voltage peak can be calculated by (38) at the frequency of f_D.

$$U_{\max,est}(f_D)[db\mu V] = 20.\log(\frac{U_{meas}}{m'^a}.\frac{1}{\mu V}) \quad (38)$$

Where $U_{max,est}$ is the estimated maximum EMI noise. However, a = 2 for the case of the triangular input current shape and m can be calculated by using

$$m' = ceil(\frac{150\,kHz}{n.f_S}) \quad (39)$$

III. Comparative Results

In order to verify the proposed modeling approach, a single-phase boost PFC converter with one stage DM EMI filter is considered. Table I presents the applied system specification. Notably, for both case studies of f_{sw} = 20 kHz and 40 kHz, the boost inductor is sized to ensure the converter's CCM operation. Two simulation cases are examined to confirm the 9–150 kHz EMI measurement of the PFC rectifier with different switching frequencies. In order to evaluate the analytical time-frequency domain estimation, simulation results, which represent real switching model of the converter are obtained in PLECS software. Finally, experimental EMI measurements are performed using ESH2-Z5 LISN and A Keysight N9010A spectrum analyzer equipped and updated with CISPR measurement requirement. Here, besides two different switching frequencies case studies, the estimated DM noise is investigated with and without EMI filter effect.

Fig. 16 illustrates the obtained comparative DM noise results for the single-phase boost PFC operating at f_{sw} = 20 kHz without the EMI filter. The obtained results show a good agreement between the proposed analytical approach and experimental results, while the conventional approach provides a reasonable estimation only for the first peak. This clearly indicates that the conventional analytical method is useful for filter design but not suitable for characterizing the converter for the entire frequency range of 9- 150 kHz. Notably, Table II summarizes the comparative DM noise results for two case studies with switching frequencies of 20 and 40 kHz without EMI filter for further comparison. As it can be seen, the proposed analytical model accurately matches the experimental results, and the maximum error in the range of 9- 150 kHz is below 1.8 dB for both considered switching frequencies. Although the conventional method has a low error at the first peak, which is enough to EMI filter design, but the error increases dramatically after the first peak.

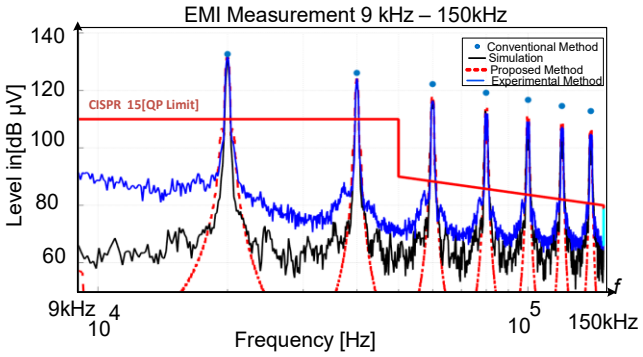

Fig. 16. Obtained DM noise for the single-phase boost PFC with f_{sw} = 20 kHz without EMI filter, based on proposed (32) and conventional (38) approaches, including PLECS simulation and experimental results.

It is clear that from Fig. 16, that both estimated and measured noise levels are exceeding the considered standard limit of CISPR 15. Hence, the EMI filter can be designed following (33) and (34) considering recommended standards limitation (e.g., here CISPR 15). Taking into account the obtained results in Table II, the first peak is used for calculating the required filter attenuation (33). Table III, illustrates the calculated DM filter parameters for both studied switching frequencies. In the following, Fig. 17 illustrates the obtained comparative results with the proposed analytical approach with f_{sw} = 20 kHz. It is clear that the designed EMI filter suitably damping the noise level to be below the standard limit. Fig. 18 shows the obtained comparative results with f_{sw} = 40 kHz. From both illustrated results in Figs. 17 and 18, it is clear that the proposed analytical approach can estimate the noise level accurately. Notably, the effect of CM noise is nullified by placing a sufficient CM filter.

TABLE II
OBTAINED COMPARATIVE DM NOISE RESULTS FOR STUDIED CASES WITHOUT EMI FILTER INCLUDED

f_{sw} = 20 kHz (CCM OPERATION)							
METHOD [dBμV]/ FREQUENCY[kHz]	20 kHz	40 kHz	60 kHz	80 kHz	100 kHz	120 kHz	140 kHz
PROPOSED	131.9	124.5	117.7	113.9	110.8	108.4	106
SIMULATED	131.3	123.1	116.4	112.8	108.7	106.4	104.5
CONVENTIONAL	132.7	126	122.1	119.2	116.7	114.6	112.7
EXPERIMENT	132.1	124	116.3	112.1	109.2	107.4	104.8
$E_{P\text{-}E}$	0.2	0.5	1.4	1.8	1.6	1	1.2
$E_{S\text{-}E}$	0.8	0.9	0.1	0.7	0.5	1	0.3
$E_{C\text{-}E}$	0.6	2	5.8	7.1	7.5	7.2	7.9
f_{sw} = 40 kHz (CCM OPERATION)							
METHOD [dBμV]/ FREQUENCY[kHz]	40 kHz	80 kHz	120 kHz	-	-	-	-
PROPOSED	136.5	128.9	121.6	-	-	-	-
SIMULATED	135.8	127	120.4	-	-	-	-
CONVENTIONAL	136.7	129.8	125.3	-	-	-	-
EXPERIMENT	135.7	128.3	119.9				
$E_{P\text{-}E}$	0.8	0.6	1.7	-	-	-	-
$E_{S\text{-}E}$	0.1	1.3	0.5	-	-	-	-
$E_{C\text{-}E}$	1	1.5	5.4				

$E_{P\text{-}E}$: Error between proposed and experimental
$E_{S\text{-}E}$: Error between simulation and experimental
$E_{C\text{-}E}$: Error between conventional and experimental

TABLE III
SPECIFICATION OF ONE-STAGE EMI FILTER AND ONE-STAGE DAMPING-STAGE.

f_{sw}	C_{DM}	R_{DM}	L_{DM}
20 KHZ	1.7 μF	22 Ω	180 μH
40 KHZ	1.3 μF	22 Ω	180 μH

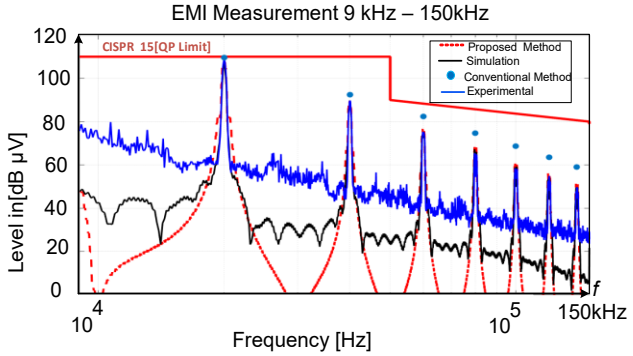

Fig. 17. Obtained DM noise results for the single-phase boost PFC with f_{sw} = 20 kHz including one-stage DM EMI filter, based on proposed (32) and conventional analytical (38) approaches, simulation-based PLECS software and experimental measurement.

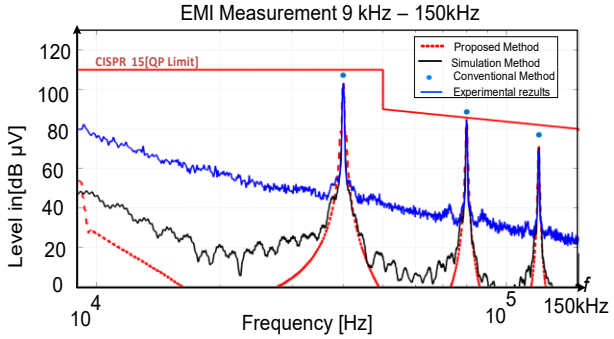

Fig. 18. Obtained DM noise results for the single-phase boost PFC with f_{sw} = 40 kHz including one-stage DM EMI filter, based on proposed (32) and conventional analytical (38) approaches, simulation-based PLECS software and experimental measurement.

TABLE IV.
OBTAINED COMPARATIVE DM NOISE RESULTS FOR STUDIED CASES WITH EMI FILTER INCLUDED

f_{sw} = 20 kHz (CCM OPERATION)							
METHOD [dBμV]/ FREQUENCY[kHz]	20 KHZ	40 KHZ	60 KHZ	80 KHZ	100 KHZ	120 KHZ	140 KHZ
PROPOSED	107.9	89.7	76.5	67.8	60.8	56	51
SIMULATED	107.1	88.3	75.3	67	59.3	54	49.8
CONVENTIONAL	109.6	92.5	82.35	74.8	68.65	63.5	59
EXPERIMENT	108.5	89.8	75.2	65.9	58.9	55.1	49.7
$E_{P\text{-}E}$	0.6	0.1	1.3	1.9	1.9	0.9	1.3
$E_{S\text{-}E}$	1.4	1.5	0.1	1.1	0.4	1.1	0.1
$E_{C\text{-}E}$	1.1	2.7	7.15	8.9	9.75	8.4	9.3
f_{sw} = 40 kHz (CCM OPERATION)							
METHOD [dBμV]/ FREQUENCY[kHz]	40 KHZ	80 KHZ	120 KHZ	-	-	-	-
PROPOSED	103.7	85	71.2	-	-	-	-
SIMULATED	103.2	83.5	70.3	-	-	-	-
CONVENTIONAL	107.2	88.6	77	-	-	-	-
EXPERIMENT	102.8	84.5	69.4				
$E_{P\text{-}E}$	0.9	0.5	1.8	-	-	-	-
$E_{S\text{-}E}$	0.4	1	0.9	-	-	-	-
$E_{C\text{-}E}$	4.4	4.1	7.6				

Finally, Table IV summarizes the outcomes of DM EMI noise for all method and the error of all them in comparison with experimental results for 20 kHz and 40 kHz. The predicted EMI noise levels from the proposed model are in well agreement with the experimental results, and the error is less than 1.9 dB at 20 kHz and 1.8 dB at 40 kHz.

IV. CONCLUSION

In this paper, an analytical time-frequency modeling approach for predicting low-frequency differential mode EMI noise is proposed. The proposed analytical approach is investigated on a single-phase PFC converter. The effectiveness of the proposed approach is demonstrated through simulation and experiments under different switching frequency operation. Moreover, the performance of this method is compared against the conventional method. Based on the provided simulations and experimental results, both proposed and conventional methods can be utilized in EMI filter design as it shows low estimation error in the first peak of the noise level. However, the proposed analytical approach shows good estimation for the entire frequency range of 9 – 150 kHz, which makes it a suitable choice for system-level investigation where only the first noise is not the purpose of the study. Finally, through the proposed modeling scheme, it is possible to identify salient features for further model order reduction and less dependency of the model

on the applied control parameters. Considering the significance of the new frequency range of 9 - 150 kHz, further study on three-phase and multi-converter-based systems is required to understand the system's frequency behavior and consequently find feasible solutions.

REFERENCES

[1] G. F. Bartak and A. Abart, "EMI of emissions in the frequency range 2 kHz–150 kHz," *22nd International Conference and Exhibition on Electricity Distribution (CIRED 2013)*, Stockholm, 2013, pp. 1-4.

[2] D. Heirman, "EMC Standards Activity," IEEE Electromagn. Compat. Mag., vol. 3, no. 1, pp. 96-99, 1st Quarter 2014.

[3] IEC TS 62578, Power electronics systems and equipment - Operation conditions and characteristics of active infeed converter (AIC) applications including design recommendations for their emission values below 150 kHz, 2015.

[4] Assessment of conducted disturbances above 2 kHz in MV and LV power systems, Cigre, reference 799, April 2020.

[5] Irish Standard Recommendation, S.R. CLC/TR 50627, Technical Report, Study Report on Electromagnetic Interference between Electrical Equipment/Systems in the Frequency Range Below 150kHz, 2015.

[6] IEC 61000-6-3:2020, Electromagnetic compatibility (EMC) - Part 6-3: Generic standards - Emission standard for equipment in residential environments, 2020.

[7] C.I.S.P.R., Specification for Radio Interference Measuring Apparatus and Measurement Methos, Publication 16, 2015, p. IEC Int. Special Committee on Radio Interference.

[8] P. Davari, F. Blaabjerg, E. Hoene, and F. Zare, "Improving 9-150 kHz EMI Performance of Single-Phase PFC Rectifier," *CIPS 2018; 10th International Conference on Integrated Power Electronics Systems*, Stuttgart, Germany, 2018, pp. 1-6.

[9] D. O. Boillat, F. Krismer and J. W. Kolar, "EMI Filter Volume Minimization of a Three-Phase, Three-Level T-Type PWM Converter System," in *IEEE Transactions on Power Electronics*, vol. 32, no. 4, pp. 2473-2480, April 2017.

[10] H. Bishnoi, A. C. Baisden, P. Mattavelli and D. Boroyevich, "Analysis of EMI Terminal Modeling of Switched Power Converters," in *IEEE Transactions on Power Electronics*, vol. 27, no. 9, pp. 3924-3933, Sept. 2012.

[11] J. Espina, J. Balcells, A. Arias, C. Ortega and N. Berbel, "EMI model of an AC/AC power converter," *2010 IEEE Vehicle Power and Propulsion Conference*, Lille, 2010, pp. 1-6.

[12] M. Hartmann, H. Ertl and J. W. Kolar, "EMI Filter Design for a 1 MHz, 10 kW Three-Phase/Level PWM Rectifier," in *IEEE Transactions on Power Electronics*, vol. 26, no. 4, pp. 1192-1204, April 2011.

[13] F. Yang, X. Ruan, Q. Ji and Z. Ye, "Input Differential-Mode EMI of CRM Boost PFC Converter," in *IEEE Transactions on Power Electronics*, vol. 28, no. 3, pp. 1177-1188, March 2013.

[14] H. Huang, L. Deng, B. Hu and G. Wei, "Techniques for Improving the High-Frequency Performance of the Planar CM EMI Filter," in *IEEE Transactions on Electromagnetic Compatibility*, vol. 55, no. 5, pp. 901-908, Oct. 2013.

[15] M. L. Heldwein and J. W. Kolar, "Design of minimum volume EMC input filters for an ultra compact three-phase PWM rectifier," *in Proc. 9th COBEP*, Sep. 30–Oct. 4, 2007. [CD-ROM].

[16] C.I.S.P.R., Limits and methods of measurement of radio disturbance characteristics of electrical lighting and similar equipment Interference, vol. 15, 2015, IEC Int. Special Committee on Radio Interference.

[17] IEC Int. Special Committee on Radio, C.I.S.P.R., Electromagnetic compatibility - Requirements for household appliances, electric tools and similar apparatus - Part 1: Emission, vol. 14. 2016, p. IEC Int. Special Committee on Radio Interference.

[18] E. O. A. Larsson, M. H. J. Bollen, M. G. Wahlberg, C. M. Lundmark and S. K. Rönnberg, "Measurements of High-Frequency (2–150 kHz) Distortion in Low-Voltage Networks," in *IEEE Transactions on Power Delivery*, vol. 25, no. 3, pp. 1749-1757, July 2010.

[19] P. Kotsampopoulos *et al.*, "EMC Issues in the Interaction Between Smart Meters and Power-Electronic Interfaces," in *IEEE Transactions on Power Delivery*, vol. 32, no. 2, pp. 822-831, April 2017.

[20] M. Klatt, R. Stiegler, J. Meyer, P. Schegner,"Generic frequency-domain model for the emission of PWM-based power converters in the frequency range from 2 to 150 kHz,"*IET* Generation*, Transmission & Distribution*, Volume: 13, Issue: 24, pp. 12 -17, 2019.

[21] Matthias Klatt, Franziska Kalse, C. L. C. Gassner, J. Meyer, P. Schegner, " Measurement and simulation of supraharmonic resonances in public low voltage networks," *25th International Conference on Electricity Distribution* Madrid, 3-6 June 2019.

[22] N. N. Esfetanaj; S. Peyghami; H. Wang; P. Davari, " Analytical Modeling of 9-150 kHz EMI in Single-Phase PFC Converter," IECON 2019 - 45th Annual Conference of the IEEE Industrial Electronics Society, Lisbon, Portugal, 2019.

[23] A. Ganjavi, H. Rathnayake, F. Zare, D. Kumar, J. Yaghoobi, P. Davari, A. Abbosh, "Common-Mode Current Prediction and Analysis in Motor Drive Systems for the New Frequency Range of 2–150 kHz," *IEEE journal Of Energing and Selected Toics in Power Elecronics*, 10.1109/JESTPE.2020.3006878.

[24] CLC/TR 50627, Study report on Electromagnetic Interference between Electrical Equipment/Systems in the Frequency Range Below 150 kHz, Ed. 2, 2014.

[25] Electromagnetic Compatibility (EMC) Part 3-2: Limits—Limits for Harmonic Current Emissions (Equipment Input Current ≤ 16 A per Phase), I. I. E. Commission, Geneva, Switzerland, 2001. Consol. Ed. 2.1.

[26] K. Raggl, T. Nussbaumer and J. W. Kolar, "Guideline for a Simplified Differential-Mode EMI Filter Design," in *IEEE Transactions on Industrial Electronics*, vol. 57, no. 3, pp. 1031-1040, March 2010.

[27] F. Costa and D. Magnon, "Graphical analysis of the spectra of EMI sources in power electronics," in *IEEE Transactions on Power Electronics*, vol. 20, no. 6, pp. 1491-1498, Nov. 2005.

[28] D. G. Holmes, T. A. Lipo, "Pulse Width Modulation for Power Converters: Principles and Practice," *IEEE Press & Wiley*, New York, NY (2003).

[29] Jian Sun, "Input impedance analysis of single-phase PFC converters," in *IEEE Transactions on Power Electronics*, vol. 20, no. 2, pp. 308-314, March 2005.

[30] G. Spiazzi and J. A. Pomilio, "Interaction between EMI filter and power factor preregulators with average current control: analysis and design considerations," in *IEEE Transactions on Industrial Electronics*, vol. 46, no. 3, pp. 577-584, June 1999.

[31] R. D. Middlebrook, "Null double injection and the extra element theorem," in *IEEE Transactions on Education*, vol. 32, no. 3, pp. 167-180, Aug. 1989.

Naser Nourani Esfetanaj (S'19) received the B.Sc. degrees in Faculty of Electrical & Computer Engineering from Tabriz University, Tabriz, Iran, in 2011 and MSC from the Faculty of Electrical Engineering from Sahand University of Technology, Tabriz, Iran in 2013. From 2013 to 2018, he was the high voltage engineer expert with MONA Consultants company, where he was responsible for the design and determining specifications of HV equipment (out-door & indoor use) in 63 to 400kV substations. He is currently working toward a Ph.D. degree in power electronic systems with the Department of Energy Technology, Aalborg University, Aalborg, Denmark. He was a visiting scholar with the power quality research group at the Faculty of Electrical Engineering and Information Technology, Dresden University of Technology, Dresden, Germany from October 2020 to December 2020. His main research interests include EMI/EMC in grid-connected converters and systems and smart grid.

Huai Wang (M'12-SM'17) received a BE degree in electrical engineering from Huazhong University of Science and Technology, Wuhan, China in 2007 and a PhD degree in power electronics from the City University of Hong Kong in 2012. He is currently Professor with the Center of Reliable Power Electronics (CORPE), Department of Energy Technology at Aalborg University, Denmark. He was a Visiting Scientist with the ETH Zurich, Switzerland, from Aug. to Sep. 2014, and with the Massachusetts Institute of Technology (MIT), USA, from Sep. to Nov. 2013. He was with the ABB Corporate Research Center, Switzerland in 2009. His research addresses the fundamental challenges in modelling and validation of power electronic component failure mechanisms and application issues in system-level predictability, condition monitoring, circuit architecture, and robustness design.

Dr. Wang received the Richard M. Bass Outstanding Young Power Electronics Engineer Award from the IEEE Power

Electronics Society in 2016, and the Green Talents Award from the German Federal Ministry of Education and Research in 2014. He is currently the Chair of IEEE PELS/IAS/IES Chapter in Denmark. He serves as an Associate Editor of IET Electronics Letters, IEEE JOURNAL OF EMERGING AND SELECTED TOPICS IN POWER ELECTRONICS, and IEEE TRANSACTIONS ON POWER ELECTRONICS.

Frede Blaabjerg (S'86–M'88–SM'97–F'03) was with ABB-Scandia, Randers, Denmark, from 1987 to 1988. From 1988 to 1992, he got the PhD degree in Electrical Engineering at Aalborg University in 1995. He became an Assistant Professor in 1992, an Associate Professor in 1996, and a Full Professor of power electronics and drives in 1998. From 2017 he became a Villum Investigator. He is honoris causa at University Politehnica Timisoara (UPT), Romania and Tallinn Technical University (TTU) in Estonia.

His current research interests include power electronics and its applications such as in wind turbines, PV systems, reliability, harmonics and adjustable speed drives. He has published more than 600 journal papers in the fields of power electronics and its applications. He is the co-author of four monographs and editor of ten books in power electronics and its applications.

He has received 33 IEEE Prize Paper Awards, the IEEE PELS Distinguished Service Award in 2009, the EPE-PEMC Council Award in 2010, the IEEE William E. Newell Power Electronics Award 2014, the Villum Kann Rasmussen Research Award 2014, the Global Energy Prize in 2019 and the 2020 IEEE Edison Medal. He was the Editor-in-Chief of the IEEE TRANSACTIONS ON POWER ELECTRONICS from 2006 to 2012. He has been Distinguished Lecturer for the IEEE Power Electronics Society from 2005 to 2007 and for the IEEE Industry Applications Society from 2010 to 2011 as well as 2017 to 2018. In 2019-2020 he served as a President of IEEE Power Electronics Society. He has been Vice-President of the Danish Academy of Technical Sciences.

He is nominated in 2014-2020 by Thomson Reuters to be between the most 250 cited researchers in Engineering in the world.

Pooya Davari (S'11–M'13-SM'19) received the B.Sc. and M.Sc. degrees in electronic engineering from University of Mazandaran (Noushirvani), Iran, in 2004 and 2008, respectively, and the Ph.D. degree in power electronics from QUT, Australia, in 2013. From 2005 to 2010, he was involved in several electronics and power electronics projects as a Development Engineer. From 2013 to 2014, he was with QUT, as a Lecturer. He joined Aalborg University, in 2014, as a Postdoc, where he is currently an Associate Professor.

He has been focusing on EMI, power quality and harmonic mitigation analysis and control in power electronic systems. He has published more than 140 technical papers. Dr. Davari served as a Guest Associate Editor of IET journal of Power Electronics, IEEE Access Journal, Journal of Electronics and Journal of Applied Sciences. He is an Associate Editor of Journal of Power Electronics, Associate Editor of IET Electronics, and Journal of Applied Sciences. He is member of the International Scientific Committee (ISC) of EPE (ECCE Europe) and a member of Joint Working Group six and Working Group eight at the IEC standardization TC77A. Dr. Davari is the recipient of a research grant from the Danish Council of Independent Research (DFF-FTP) in 2016, and 2020 IEEE EMC Society Young Professional Award for his contribution to EMI and Harmonic Mitigation and Modeling in Power Electronic Applications. He is currently Editor-in-Chief of Circuit World Journal.